CHAPTER 3

METHODOLOGY

Sample Preparation

The polycrystalline sample of GST was bought from rare-metal material company, China. The cylindrical ingots sample had dimensions of 38.15 x 5.02 mm^2. The bulk density was measured using the standard Archimedes method.

Phase Formation and Chemical Composition Analysis

For study behavior on melting temperature of GST we were using Thermogravimetric differential thermal analysis (TG-DTA) and the elemental compositions of GST were determined using energy-dispersive X-ray spectroscopy (EDX) was done on at an accelerating voltage of 15 keV. The following methods were used:

Thermogravimetry and Differential Thermal Analysis

Thermogravimetry analysis (TGA) and differential thermal analysis (DTA) are the technique measuring the variation in mass of a sample when it is subjected to a constant heating rate in a controlled atmosphere (Hitachi High-Tech Science Exstar TG/DTA series 7200). This variation in mass can be either a mass loss (vapor emission) or mass gain (gas fixation). The measurement of the mass of the sample as a function of temperature reveals its purity, decomposition behavior, and chemical kinetics. The temperature difference between reference and simple is monitored as a function of temperature. The schematic diagram of TG-DTA system is shown in Figure 9.

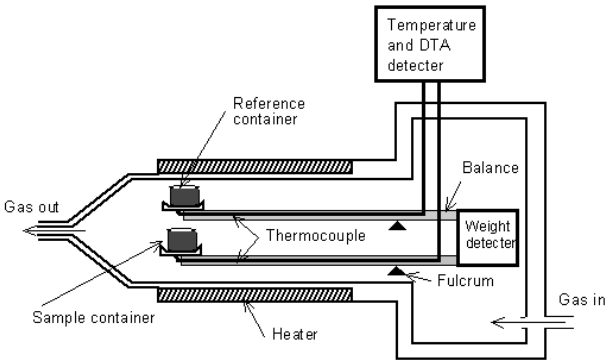

Figure 9 Schematic diagram of the TG–DTA system (Murasawa, Koseki, Li, Iwata, & Sakamoto, 2012)

Figure 10 Show TG–DTA measurement at Osaka Prefecture University

The sample was performed on ~10 mg of sample sealed inside evacuated aluminum oxide (Al_2O_3) container. The sample was heated from room temperature to 1273 K with a heating/cooling rate of 293 K min^{-1}.

Energy Dispersive X-ray Spectroscopy

Energy Dispersive X-ray spectroscopy (EDX) is a micro-analytical technique that uses the characteristic spectrum of X-rays emitted by the specimen after excitation by high-energy electrons to obtain information about its elemental composition. The EDX analysis here was performed on a Field Emission Scanning Electron Microscopy JSM-7001F (FE-SEM).

Sample Identification

We identifications a sample was made carried out using the X-ray diffraction (XRD) technique.

X-ray Diffraction Analysis

The X-ray diffraction (XRD) measurements was performed on Rigaku Smart Lab at Osaka Prefecture University; Japan and Center of Excellence on Alternative Energy at Sakon Nakhon Rajabhat University; Thailand by using Cu-Kα1 radiation at room temperature (λ = 1.5406 Å). The characteristic x-ray diffraction pattern generated in a typical XRD analysis provides a unique "fingerprint" of the crystals present in the sample. When properly interpreted, by comparison with standard reference patterns and measurements, this fingerprint allows identification of the crystalline form. When a focused X-ray beam interacts with these planes of atoms, part of the beam is transmitted, part is absorbed by the sample, part is refracted and scattered, and part is diffracted. Diffraction of an X-ray beam by a crystalline solid is analogous to diffraction of light by droplets of water, producing the familiar rainbow. X-rays are diffracted by each mineral differently, depending on what atoms make up the crystal lattice and how these atoms are arranged (Pandian, 2014). These result in diffraction in which X-rays are emitted at characteristic angles based on the spaces between the atomic planes in the crystal structure. Most crystals have many sets of planes passing through their atoms. Each set of planes has a specific

interlunar distance and will give rise to a characteristic angle for diffracted X-rays. The basic principle of XRD is Bragg's law, see Figure 11, given by;

$$2d_{hkl}\sin\theta = n\lambda \qquad (3.1)$$

Where d, θ, λ, and n are lattice spacing, diffraction angle, the wavelength of the X-ray, and an integral number respectively. A set of 'd-spaces' obtained from a single compound will represent the set of planes that can pass through the atoms and can be used for comparison with sets of d-spaces obtained from standard compounds (Overview, 2013)

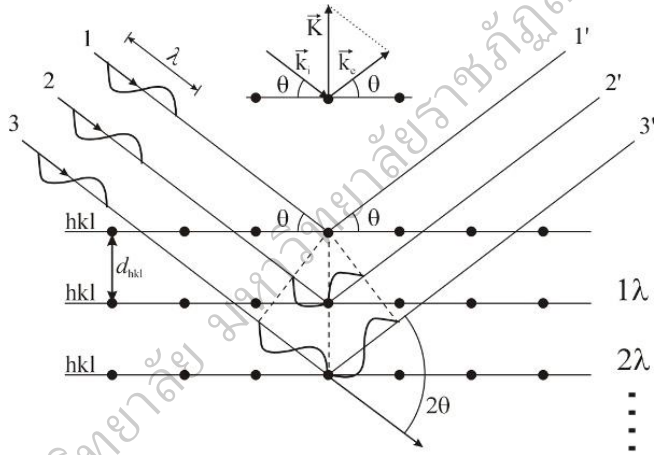

Figure 11 Diffraction (i.e. constructive interference of the scattered X-rays) will occur if the Bragg condition (eq. 3.1) is fulfilled and of the scattering vector K is parallel to the normal of the hkl-planes. (Myers, 2002)

มหาวิทยาลัย มหาวิทยาลัยราชภัฏสกลนคร

Figure 12 the X-ray diffraction (XRD) measurements was performed on (left) Rigaku Smart Lab at Osaka Prefecture University and (right) Center of Excellence on Alternative Energy at Sakon Nakhon Rajabhat University

Surface Microstructure

The surface microstructure measurement was revealed by the Field Emission Scanning Electron Microscopy SU8000 (FE-SEM).

Field Emission Scanning Electron Microscopy

Field emission scanning electron microscopy (FESEM) provides topographical and elemental information at magnifications of 10x to 300,000x, with virtually unlimited depth of field. Compared with convention scanning electron microscopy (SEM), field emission SEM (FESEM) produces clearer, less electrostatically distorted images with spatial resolution down to 1 1/2 nanometers – three to six times better. The FE-SEM observations

were performed on a Hitachi Ultra-high Resolution Scanning Electron Microscope SU8000. The schematic diagram of the FE-SEM equipment is shown in Figure 13.

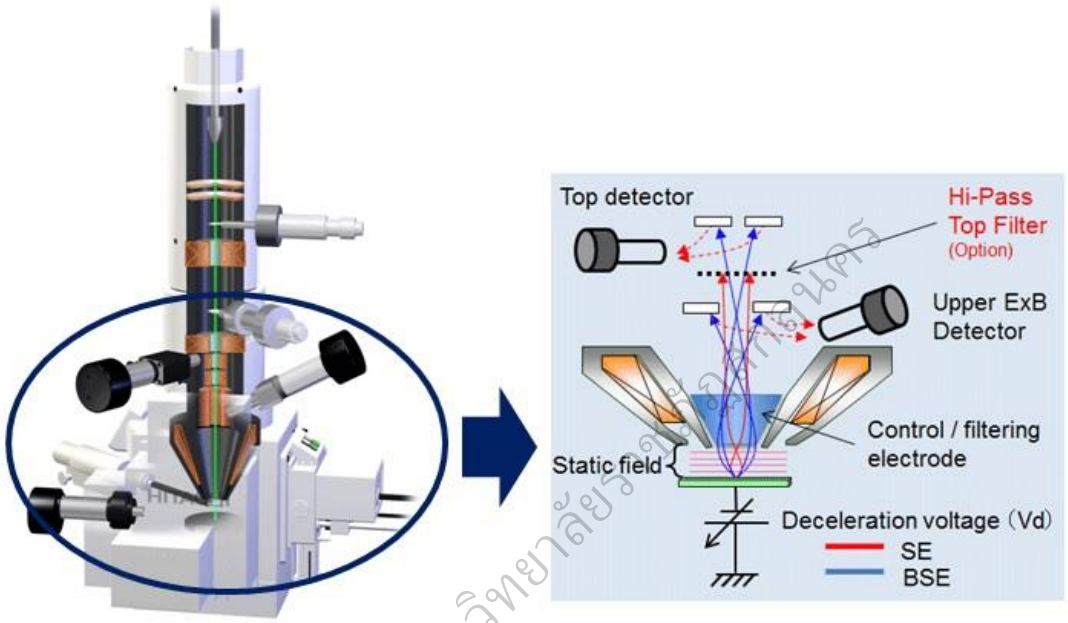

Figure 13 Schematic diagram of the FE-SEM equipment

[http://www.hitachi-hightech.com]

Figure 14 The FE-SEM observations were performed on a Hitachi Ultra-high Resolution Scanning Electron Microscope SU8000 at Osaka Prefecture University

Vicker Hardness

The Vickers hardness was measured by micro hardness tester. The Vickers test is often easier to use than other hardness tests because can be required calculations are independent of the size of the indenter and indenter can be used for all materials irrespective of hardness. We measured GST at room temperature by micro hardness tester with varies loads of 0.01, 0.05, 0.5 N at 10 seconds, and the repeated 3 times for each sample, and the average hardness measured data. The unit of hardness of our sample given by the test is known as the Vickers Pyramid Number (HV) indenter into the surface of the specimen, defined by,

$$H_V = \frac{2P_H \sin\theta}{l^2} = 1.8544\frac{P_H}{l^2} \qquad (3.2)$$

Where l (mm) is the average diagonal length of the diamond shaped impression made on the indented surface, P_H is the stress of the indenter. The unit of the Vickers hardness can be used GPa, given by (3.2)

Figure 15 Vickers hardness tester Model at CEAE, Sakon Nakhon Rajabhat University

Electrical Resistivity and Seebeck Coefficient

Electrical Resistivity and Seebeck coefficient were measured with the standard four–probe method by using a commercially available apparatus (ZEM–3; ULVAC Technologies), at 300–710 K in helium atmosphere.

The electrical resistivity is represented by the following equation:

$$\rho = \frac{\sum z_i \sum y_i - N \sum z_i y_i}{\left(\sum z_i\right)^2 - N \sum z_i^2} \frac{wD}{L} \qquad (3.3)$$

Where y_i the probe to probe voltage is, z_i is the test electrical current, wD are the width / depth of specimen, L is the probe separation length and N is the specimen size.

The Seebeck coefficient is represented by the following equation:

$$S = -\frac{\sum x_i \sum y_i - N \sum x_i y_i}{\left(\sum x_i\right)^2 - N \sum x_i^2} + S_{wire}\left(T\right) \qquad (3.4)$$

Where x_i the probe of temperature difference is, y_i is the probe to probe voltage, S_{wire} is the wire Seebeck coefficient, N is the specimen size and T is the temperature, respectively.

บัณฑิตวิทยาลัย จุฬาลงกรณ์มหาวิทยาลัย

Figure 16 Show ZEM-3; ULVAC Technologies apparatus

Thermal Conductivity

The κ value was evaluated from the thermal diffusivity α , heat capacity C_p , and sample of density *d*, based on the relationship:

$$\kappa = \alpha C_p \mathrm{d} \qquad (3.5)$$

α and C_p were determined by the laser flash method and laser flash differential calorimetry in a vacuum, using a commercially available apparatus (FlashTE; PicoTherm) (Kosuga et al., 2015).

Figure 17 Show thermal conductivity was measured by using FlashTE; PicoTherm at Osaka University

Density

The density of GST specimen was measured using the standard Archimedes method. The density, or more precisely, the volumetric mass density, of a substance is its mass per unit volume. Mathematically, density is defined as mass divided by volume:

$$\rho = \frac{m}{V} \tag{3.6}$$

Where ρ is the density, m is the mass, and V is the volume. The SI unit of density is the kilogram per cubic meter (kg m^{-3}).

Figure 18 Show density Kit at CEAE Sakon Nakhon Rajabhat University

บัณฑิตวิทยาลัย มหาวิทยาลัยราชภัฏสกลนคร

Archimedes' Principle

Archimedes' principle aids in the experimental determination of density by providing a convenient and accurate method for determining the volume of an irregularly shaped object, like a rock. Archimedes' principle is a law of physics fundamental to fluid mechanics. It was formulated by Archimedes of Syracuse (Acott, 1999)

Dimensionless Figure of Merit

The dimensionless figure of merit (ZT) was calculated by using the above mentioned values of the Seebeck coefficient (S), electrical resistivity (ρ) and thermal conductivity (κ), consider by the relation (Rowe, 2005):follow as (2.13).

Calculation Thermoelectric Properties of GeTe and Sb_2Te_3

We went too investigated predict the thermoelectric properties and the effect of GeTe and Sb_2Te_3 for supported experimental data of Ge–Sb–Te material. The calculation of band structures were perform by QUANTUM ESPRESSO with involving plan wave self–consistent field (PWscf) under the scope of density functional theory (DFT) (Andrea {Dal Corso} and Stefano de Gironcoli and Stefano Fabris and Guido Fratesi and Ralph Gebauer and Uwe Gerstmann and Christos Gougoussis and Anton Kokalj and Michele Lazzeri and Layla Martin–Samos and Nicola Marzari and Francesco Mauri and Riccardo Mazzarello and Stefano Paolini and Alfredo Pasquarello and Lorenzo Paulatto and Carlo Sbraccia and Sandro Scandolo and Gabriele Sclauzero and Ari P Seitsonen and Alexander Smogunov and Paolo Umari and Renata M Wentzcovitch}, 2009). We used the PBE (Predew, Burke, and Ernzerhof), generalized gradient approximations (GGA), and Rabe Rappe Kaxiras Joannopoulos (RRKJ) ultrasoft pseudopotentials for exchange correlation potentials. The kinetic energy cutoff using 40 Ry and charge density cutoff using 160 Ry for self–consistent field. The convergence threshold we used the self–consistent method operated value 10–8 and mixing beta value is 0.7. The band structure of GeTe was calculated using 9×9×9 k–point grid, while Sb_2Te_3 using 8×8×8 k–point grid. A dense k mesh 40,000 k points was used in the Brillouin zone for GeTe and Sb_2Te_3. The thermoelectric properties composed the S, the σ , and the κ were calculated by using Boltzmann transport theory based on BoltzTraP code (Madsen & Singh, 2006).The thermoelectric properties, the S, the σ , the κ obtained by equations;

$$S_{\alpha\beta}(T,\mu) = \frac{1}{eT\sigma_{\alpha\beta}(T,\mu)} \int \bar{\sigma}_{\alpha\beta}(\varepsilon)(\varepsilon-\mu)\left[-\frac{\partial f_{\mu}(T,\varepsilon,\mu)}{\partial\varepsilon}\right] d\varepsilon \qquad (3.8)$$

$$\sigma_{\alpha\beta}(T,\mu) = \frac{1}{\Omega} \int \sigma_{\alpha\beta}(\varepsilon)\left[-\frac{\partial f_{\mu}(T,\varepsilon)}{\partial\varepsilon}\right] d\varepsilon \qquad (3.9)$$

$$\kappa_{\alpha\beta}^{0}(T;\mu)=\frac{1}{e^{2}T\Omega}\int\sigma_{\alpha\beta}(\varepsilon)(\varepsilon-\mu)^{2}\left[-\frac{\partial f_{\mu}(T;\varepsilon)}{\partial\varepsilon}\right]d\varepsilon \tag{3.10}$$

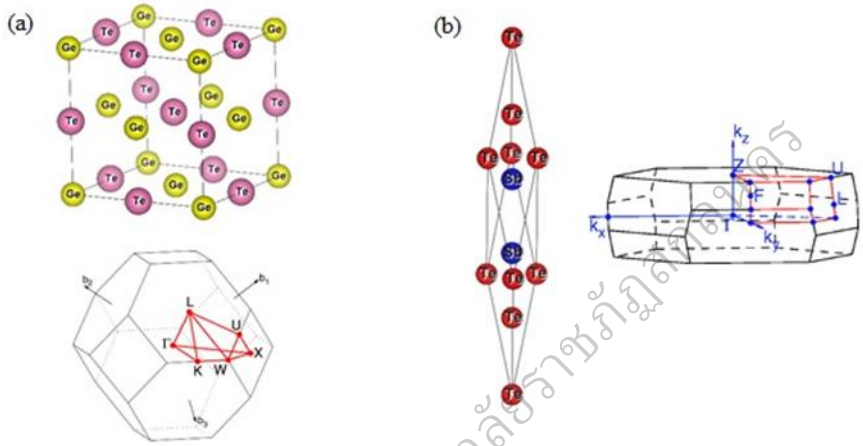

Figure 19 Crystal structure and the Brillouin zone of (a) GeTe face centered cubic lattice (Setyawan & Curtarolo, 2010) and (b) Sb_2Te_3 rhombohedral lattice structure (Yavorsky, Hinsche, Mertig, & Zahn, 2011).

Thermoelectric Cell and Module

A thermoelectric module is a circuit containing thermoelectric materials that generate electricity from heat directly. In this case, we used thermoelectric module consists of only one type used to construct a thermoelectric module. A direct electric current will flow in the circuit when there is a temperature difference between the materials. Generally, the current magnitude has a proportional relationship with the temperature difference. (i.e., the more the temperature difference, the higher the current.) In application, thermoelectric modules in power generation work in very tough

mechanical and thermal conditions. Because they operate in very high temperature gradient, the modules are subject to large thermally induced stresses and strains for long periods of time. They also are subject to mechanical fatigue caused by large number of thermal cycles. Thus, the junctions and materials must be selected so that they survive these tough mechanical and thermal conditions. The efficiency of thermoelectric modules are greatly affected by its geometrical design.

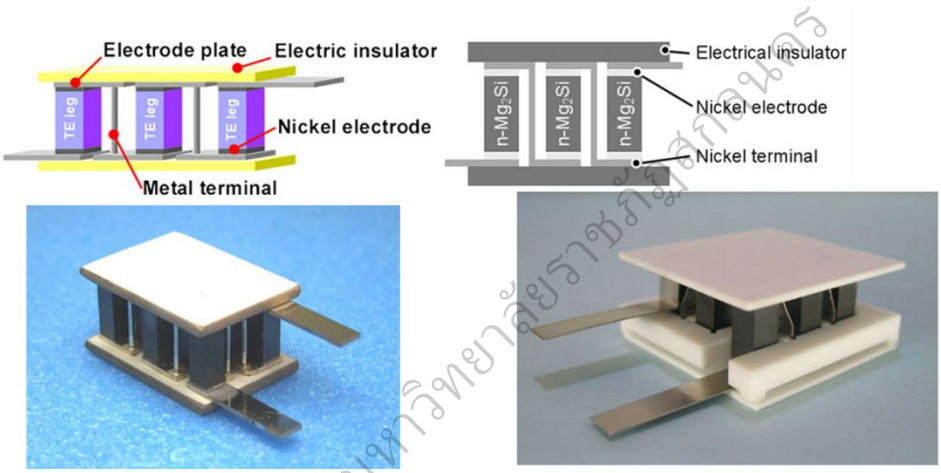

Figure 20 Construct of uni-legs thermoelectric module (Nemoto et al., 2012)

มหาวิทยาลัยราชภัฏสกลนคร

Fabrication of the Thermoelectric Unileg Cell

The process of fabricated thermoelectric unileg cell by using GST bulk material. Cutting a GST material were 2 × 2 × 2.5 mm^3 for making unileg cell. Ultrasonic Soldering method were formed in order to create a good contact between the element and the metal parts in the cell or module. Firstly, we including soldering copper wire on top and bottom of GST bulk material. The thickness of the soldering copper wire was about 0.2 mm. Next, the unileg cell is constructed by connecting in series with thin copper and wire electrodes using solder connected on top and bottom to an alumina substrate. The substrate used alumina plate size 1×1 cm^2. Then the cell cooled at room temperature

connected red and black wire for two legs, respectively then test power and failure temperature for limit temperature used for TE cell.

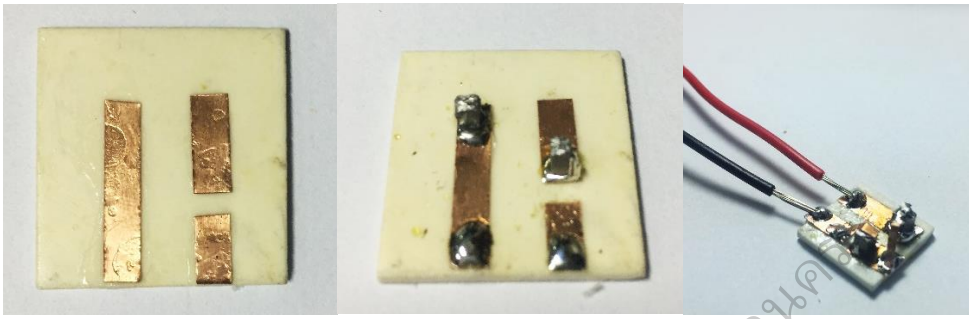

Figure 21 Show process of fabrication the GST unileg cell

Fabrication of the Thermoelectric Module

Cutting a GST material were 2 × 2 × 2.5 mm^3 for making module. In this work, we using only one type for innovated module. The GST legs have 16 pairs on alumina substrate plate size 2.54 × 2.54 cm^2. The TE module is constructed by connecting in series with thin copper and soldering copper wire electrodes for connected on top and bottom. Then the cell cooled at room temperature connected red and black wire for two legs, respectively then test power and failure temperature for limit temperature used for TE cell. After that, we took the GST–unileg to measure voltage values.

บัณฑิตวิทยาลัย มหาวิทยาลัยราชภัฏจันทรเกษม

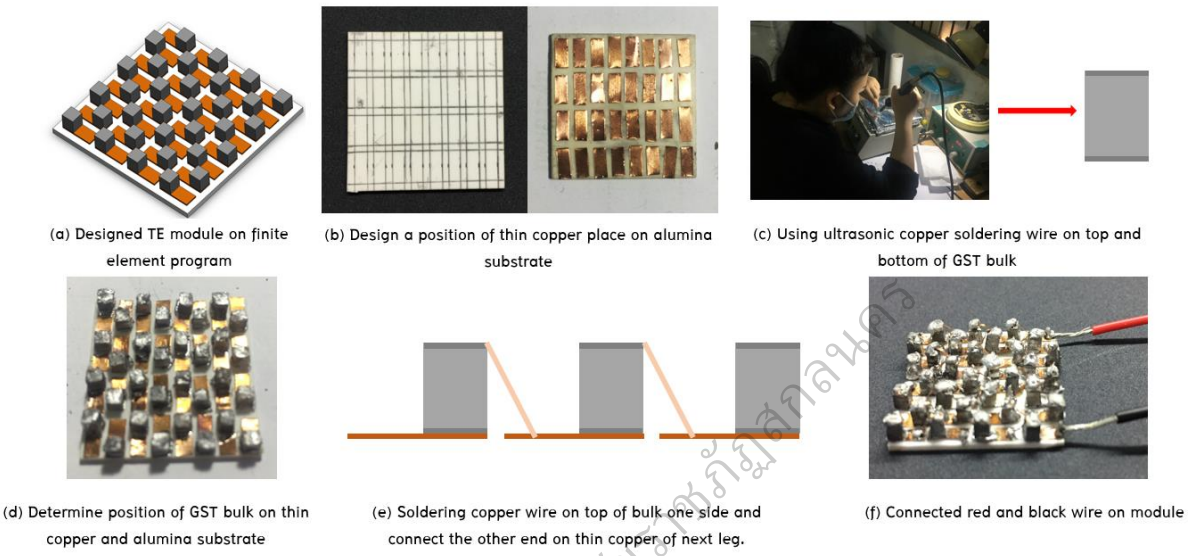

Figure 22 Shows diagram of fabrication TE–GST module

Power Generation Measurement of Thermogenerator

The power generation of thermgenerator described above were installed over a heater, and a water cooling was placed over the module. To measure the temperatures of hot and cold side temperatures, the two K–type thermocouples were attached on the thin mica plate of high temperature and low temperature sides using an alumina substrate, respectively. A photograph of output power measurement of thermoelectric module is shown in Figure 21. The output power (W) was calculated by the output voltage (V) and current (I) caused by changing a resistor.

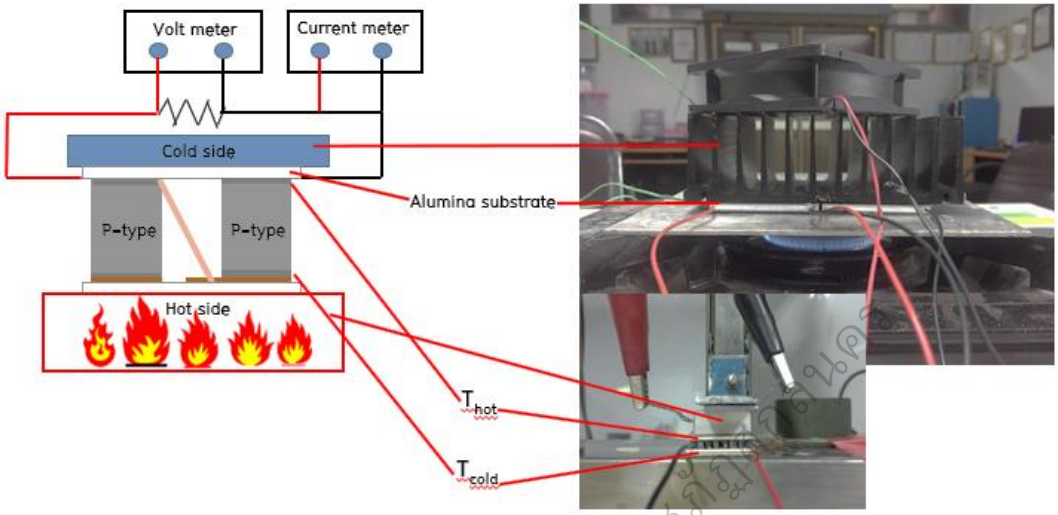

Figure 23 Shows schematic diagram how to measure power generation of thermoelectric module

In the case, we fabricated thermoelectric module from GST material for use with this work but after took to electrical power measured shows lowest electrical power values for generate electricity on lighting system. So therefore, we need to use the modules thermoelectric commercial used to generate electricity for lighting system instead of using GST-unileg thermoelectric module. The thermoelectric commercial was bought from TECTEG MFR Company, Canada. The cylindrical ingots sample had dimensions of the thermoelectric module commercial 6-8 pieces measured power generation and output voltage before install on stove fuel.

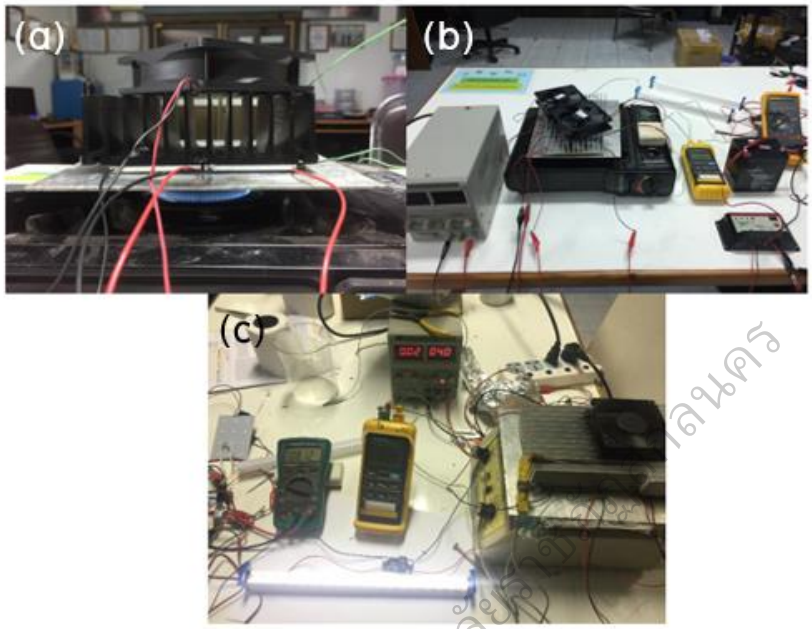

Figure 24 Shows schematic diagram how to measure power generation of thermoelectric modules commercial

The Maximum Theoretical Efficiency (Ɛ) for Conversion of Heat Transferred

From research and development of thermoelectric materials were found that the efficiency of electricity generators is properties must have followed features:

1. Can provide high conductivity, but the heat a little. (Thermal resistance caused by the flow of electric current).

2. Can convert heat into electrical energy. Or cooling energy as much as possible.

3. Has a low thermal conductivity to prevent thermal conduction through material.

$$\varepsilon = \frac{T_h - T_c}{T_h}\left[\frac{\sqrt{1+ZT}-1}{\sqrt{1+ZT}-\left(\frac{T_c}{T_h}\right)}\right] \quad (3.11)$$

Where ε is the maximum theoretical efficiency, T_h is hot side (K), T_c is cold side (K) and ZT is Dimensionless Figure of Merit (2.13).

Conversion Efficiency of Thermoelectric Cell and Module

The efficiency of a thermoelectric converter depends heavily on the temperature difference $\Delta T = T_h - T_c$ across the device. This is because the thermoelectric generator, like all heat engines, cannot have an efficiency greater than that of a Carnot cycle $\left(\Delta T / T_h\right)$. The efficiency of a thermoelectric generator is typically defined as (Snyder, 2008)

$$\eta = \frac{\Delta T}{T_h}\cdot\frac{\sqrt{1+ZT}-1}{\sqrt{1+ZT}+T_c/T_h} \quad (3.12)$$

Where the first term is the Carnot efficiency and ZT is the figure of merit for the device.

บัณฑิตวิทยาลัย มหาวิทยาลัยราชภัฏสกลนคร

Thermoelectric Applications

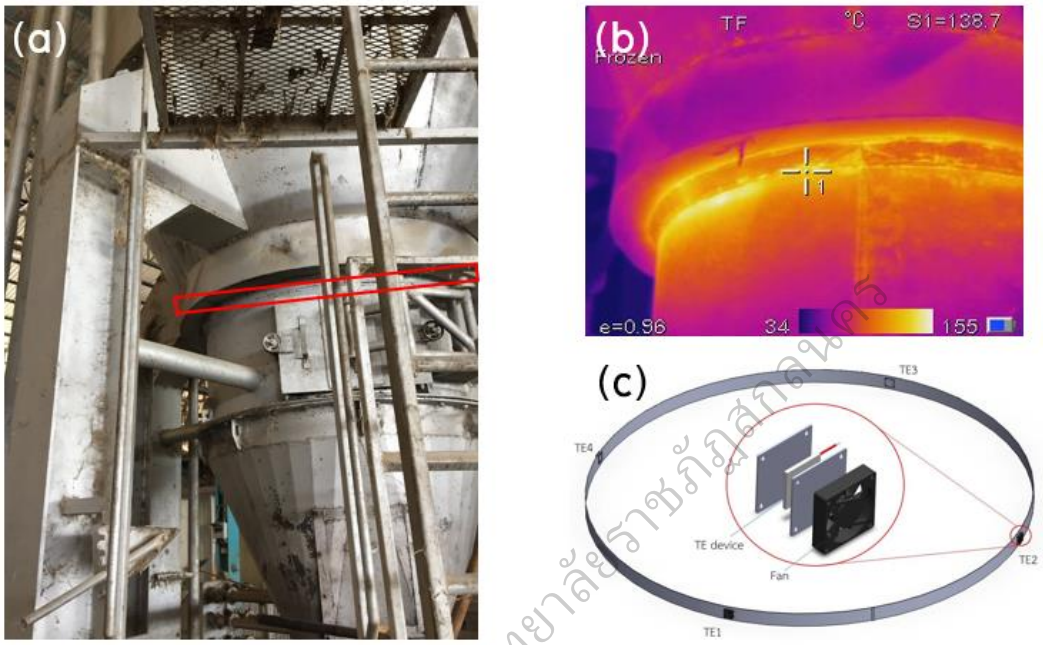

Figure 25 shows (a) the stove fuel at rice mill industry, (b) thermoscan of area on machine and (c) schematic diagram of thermogenerator system

From the proposed of thesis, we wanted to focus the heat lost from the stove fuel using a large baking on rice mill industry for generated electricity by using thermoelectric module. The baking a rice process, they use the husk to burn it for fuel. In figure 25 (b) shows thermos scan on stove fuel of rice dryer machine. We found the stove fuel has the highest heat lost around 411 K. Therefore, this area has suitable for stick the thermoelectric generator. The thermogenetor system consist of 8–10 modules, heat sink and cooling fan connected series on stainless steel. The thermogenerator were generated direct current electricity to battery for back up charge for turn on the light system.

Summary of Investigating Topics

The topics of investigation in this research can be summarized as follows.

1. Phase formation and microstructure of GST material
2. Crystal structure and chemical composition analysis
3. Surface microstructure and impression of Vickers hardness
4. Thermoelectric properties of GST material
5. Electronic structure calculation of GeTe and Sb_2Te_3
6. Thermoelectric Cell and Module

บัณฑิตวิทยาลัย มหาวิทยาลัยราชภัฏธนบุรี

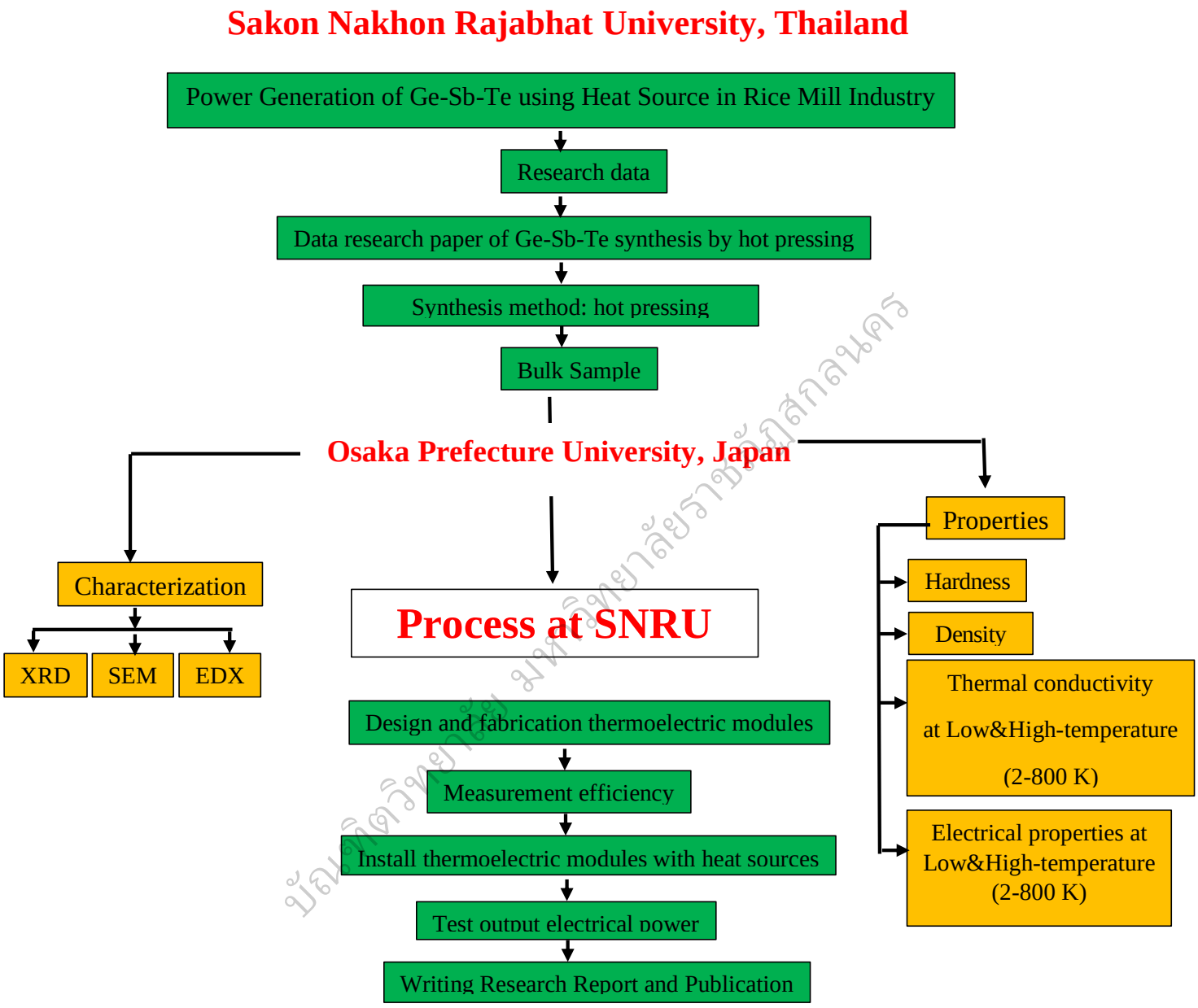

Figure 26 Show schematic diagram of thesis process

References

Acott, C. (1999). "The diving "Law-ers": A brief resume of their lives." *South Pacific Underwater Medicine Society journal, 29*(1).

Andrea {Dal Corso} and Stefano de Gironcoli and Stefano Fabris and Guido Fratesi and Ralph Gebauer and Uwe Gerstmann and Christos Gougoussis and Anton Kokalj and Michele Lazzeri and Layla Martin-Samos and Nicola Marzari and Francesco Mauri and Riccardo Mazzarello and Stefano Paolini and Alfredo Pasquarello and Lorenzo Paulatto and Carlo Sbraccia and Sandro Scandolo and Gabriele Sclauzero and Ari P Seitsonen and Alexander Smogunov and Paolo Umari and Renata M Wentzcovitch}, P. G. a. S. B. a. N. B. a. M. C. a. R. C. a. C. C. a. D. C. a. G. L. C. a. M. C. a. I. D. a. (2009). QUANTUM ESPRESSO: a modular and open-source software project for quantum simulations of materials. *Journal of Physics: Condensed Matter,, 21*, 395502 (395519pp).

Kosuga, A., Nakai, K., Matsuzawa, M., Fujii, Y., Funahashi, R., Tachizawa, T., . . . Kifune, K. (2015). Crystal structure, microstructure, and thermoelectric properties of GeSb 6 Te 10 prepared by spark plasma sintering. *Journal of Alloys and Compounds, 618*, 463-468.

Madsen, G. K., & Singh, D. J. (2006). BoltzTraP. A code for calculating band-structure dependent quantities. *Computer Physics Communications, 175*(1), 67-71.

Murasawa, N., Koseki, H., Li, X.-R., Iwata, Y., & Sakamoto, T. (2012). Study on thermal behaviour and risk assessment of biomass fuels. *International Journal of Energy Engineering, 2*(5), 242-252.

Myers, H. P. (2002). Introductory Solid State Physics. *Taylor & Francis*.

Nemoto, T., Iida, T., Sato, J., Sakamoto, T., Nakajima, T., & Takanashi, Y. (2012). Power Generation Characteristics of Mg 2 Si Uni-Leg Thermoelectric Generator. *Journal of electronic materials, 41*(6), 1312-1316.

Overview, D. D. (2013). Advanced X-ray Diffraction System for Materials Research Applications.

Pandian, M. S. (2014). X-ray Diffraction Analysis: Principle, Instrument and Applications.

Rowe, D. M. (2005). *Thermoelectrics handbook: macro to nano*: CRC press.

Setyawan, W., & Curtarolo, S. (2010). High-throughput electronic band structure calculations: Challenges and tools. *Computational Materials Science, 49*(2), 299-312. doi: http://dx.doi.org/10.1016/j.commatsci.2010.05.010

Snyder, G. J. (2008). Small thermoelectric generators. *The Electrochemical Society Interface, 17*(3), 54.

Yavorsky, B. Y., Hinsche, N. F., Mertig, I., & Zahn, P. (2011). Electronic structure and transport anisotropy of Bi${}_{2}$Te${}_{3}$ and Sb${}_{2}$Te${}_{3}$. *Physical Review B, 84*(16), 165208.

บัณฑิตวิทยาลัย มหาวิทยาลัยราชภัฏสกลนคร

บัณฑิตวิทยาลัย มหาวิทยาลัยราชภัฏสกลนคร